



Simultaneous voltammetric determination of guanine and adenine using MnO₂ nanosheets and ionic liquid-functionalized graphene combined with a permeation-selective polydopamine membrane

Shuang Zhang¹ · Xuming Zhuang¹ · Dandan Chen¹ · Feng Luan¹ · Tao He¹ · Chunyuan Tian¹ · Lingxin Chen^{1,2}

Received: 30 January 2019 / Accepted: 2 June 2019 / Published online: 13 June 2019
© Springer-Verlag GmbH Austria, part of Springer Nature 2019

Abstract

Guanine and adenine in blood samples can be detected by using an electrochemical sensor based on the use of manganese dioxide (MnO₂) nanosheets and ionic liquid functionalized graphene (IL-GR) bound to a polydopamine (PDA) membrane. Both guanine and adenine undergo a redox reaction on the surface of the modified electrode. Cyclic voltammetry and differential pulse voltammetry were used to evaluate the electrochemical behavior of a glassy carbon electrode (GCE) modified with PDA/MnO₂/IL-GR. The sensor allows for individual as well as simultaneous determination of guanine and adenine. The working voltage of differential pulse voltammetry at which data were acquired to establish the calibration plot: 0.6–1.2 V for guanine, 0.8–1.4 V for adenine, 0.4–1.4 V for mixture of guanine and adenine. A wide detection range (10–300 μM), low detection limits (guanine: 0.25 μM; adenine: 0.15 μM), selectivity and reproducibility are demonstrated. The modified GCE was successfully applied to the analysis of guanine and adenine in spiked fetal bovine serum and mouse whole blood samples.

Keywords Electrochemical · Nanocomposites · Sensor · Guanine · Adenine · Fetal bovine serum · Mouse whole blood

Introduction

In being components of both deoxyribonucleic acid (DNA) and ribonucleic acid (RNA), guanine and adenine play important roles in biochemical processes. They are involved in the processes of energy supply, metabolic regulation as well as coenzyme formation [1]. Also, they are widely considered important in regulating coronary and cerebral circulation,

controlling blood flow, preventing arrhythmias, releasing neurotransmitters, and modulating the activity of adenylate cyclase [2]. Abnormal concentrations levels of guanine and adenine may be associated with mutation of the immune system and some diseases, such as acquired immune deficiency syndrome (AIDS), human immunodeficiency virus (HIV) infection, cancers and epilepsy [3]. The levels of guanine and adenine have been proposed as markers for disease diagnosis, disease progression, and treatment responses. Hence, the accurate and fast monitoring of guanine and adenine is important in clinical medicine [4].

There are some methods being used to detect guanine and adenine, including high performance liquid chromatography (HPLC) [5], capillary electrophoresis (CE) [6], mass spectrometry (MS) [7], and electrochemical analysis [8]. Among them, electrochemical sensors has become a potential technique for guanine and adenine detection because of their simplicity, miniaturization, rapid response and low cost [9].

However, the use of electrochemical sensors to detect guanine and adenine directly in the blood often faces some problems. Due to low electron transfer and limited active surface areas, the response for the direct oxidation of guanine and adenine was poor on the bare electrode [10]. In order to

Electronic supplementary material The online version of this article (<https://doi.org/10.1007/s00604-019-3577-4>) contains supplementary material, which is available to authorized users.

✉ Xuming Zhuang
xmzhuang@iccas.ac.cn

✉ Tao He
13562512013@163.com

✉ Lingxin Chen
lxchen@yic.ac.cn

¹ College of Chemistry and Chemical Engineering, Yantai University, Yantai 264005, China

² CAS Key Laboratory of Coastal Environmental Processes and Ecological Remediation, Yantai Institute of Coastal Zone Research, Chinese Academy of Sciences, Yantai 264003, China

overcome these disadvantages, and obtain faster electron transfer and more electrochemical active sites, various nanomaterials modified electrodes have been fabricated to detect guanine and adenine. For instance, Ensafi et al. constructed a sensor based on multi-walled carbon nanotubes (MWCNTs) and NiFe_2O_4 , which can be used to test the guanine and adenine simultaneously or separately [11]. More excellent or alternative nanocomposites are necessary to be exploited in order to modify electrodes for more sensitive determination of adenine and guanine.

Graphene has some excellent characteristics, such as high conductivity, strong mechanical properties and large specific surface area, which have been proved to be suitable for building biosensors [12–15]. However, the problem of irreversible aggregation needs to be solved before the use of this material [16]. Ionic liquids (ILs) usually include pyridine salts, imidazole salts, season phosphine salts, quaternary ammonium salts, which have unique physicochemical properties such as wide electrochemical window, high ionic conductivity and good solubility. Hence, ionic liquid functionalized graphene (IL-GR) has a potential application by introducing a surface charge and avoiding the aggregation of graphene to obtain polydisperse and long-term stable IL-GR [17]. For this, Chai et al. [18] synthesized AuPd alloy nanoparticles on IL-GR by one step method. The excellent electrocatalytic performance of the sensor toward formic acid was confirmed.

Manganese dioxide (MnO_2) nanomaterials have gained extensive concerns in the field of electrochemical sensors due to their excellent properties, such as relatively high energy density, high activity, large surface area, nontoxic, environmental compatibility, low cost and natural abundance. However, MnO_2 nanomaterials have relatively high resistance, which impeding the further application of MnO_2 nanomaterials [19]. To solve this problem, MnO_2 nanomaterials tend to be combined with carbon-based materials, such as graphene, graphene oxide and carbon nanotubes to improve the conductivity and obtain a synergistic effect [20]. Majd et al. [21] constructed a non-enzymatic biosensor based on graphene/ MnO_2 nanocomposite for determination of H_2O_2 . The sensor exhibited good properties such as a low detection limit, high sensitivity, and excellent selectivity in the determination of H_2O_2 .

Nevertheless, electrochemical sensors constructed based on the above-mentioned nanomaterials often encounter severe challenges-nonspecific adsorption of proteins in the detection of actual samples (whole blood, serum, etc.), which will interfere with the sensing system and affect the signal response of the detection [22]. Polydopamine (PDA) coatings have received wide attentions as a versatile platform for application in membrane surface modification [13]. Two functions of the PDA layer of the nanocomposite membrane have been exhibited: reducing the pore sizes of nanocomposite support to reject macromolecular protein and providing reaction sites [23]. Li et al. [24] developed an electrochemical sensor for H_2O_2

based on prussian blue and carbon nanotube overcoated with a PDA membrane, which can directly perform in vivo detection of H_2O_2 without interference.

In this paper, IL-GR and MnO_2 nanosheets were prepared, combined and loaded onto the glass carbon electrode (GCE), being covered with a layer of PDA film to structure a sensitive electrochemical sensor for the detection of adenine and guanine. By combining synergistic sensitization of MnO_2 /IL-GR with selectivity of PDA film, the improvement of electrochemical performance was realized. The performance of PDA/ MnO_2 /IL-GR was assessed by electrochemical methods and the satisfactory results indicated a potential of this sensor for the simultaneous detection of guanine and adenine.

Experimental

Reagents and materials

GO was supplied by Nanjing XFNano Materials Technology Company (Nanjing, China, <https://www.xfnano.com>). All the other chemicals such as 2-bromoethylamine hydrobromide, 1-methylimidazole, $\text{MnCl}_2 \cdot 4\text{H}_2\text{O}$, tetramethyl-ammonium, $\text{K}_3\text{Fe}(\text{CN})_6$, $\text{K}_4\text{Fe}(\text{CN})_6$, ascorbic acid (AA), uric acid (UA), glucose, guanine, adenine, dopamine hydrochloride, citric acid, sodium citrate, Bull Serum Albumin (BSA), Britton-Robinson (BR) buffer and phosphate buffered solution were obtained from Sigma (Shanghai, China, <https://www.sigmaldrich.com/china-mainland.html>). Fetal bovine serum (FBS, #10439024) was purchased from Thermo Fisher Scientific (<https://www.thermofisher.com/cn/zh/home.html>). All reagents were analytical grade and used according to the instructions. Ultrapure water (18.25 $\text{M}\Omega$ cm) was used for all experiments.

Apparatus

Structural characterizations of the nanomaterials were performed using scanning electron microscopy (SEM, S-4800, Hitachi, Ltd., Japan), transmission electron microscopy (TEM, JEOL 2010F, 200 kV), Raman spectroscopy (RENISHAW A-9570-2000), and X-ray photoelectron spectroscopy (XPS, ESCALAB 250xi). Electrochemical properties were investigated on an electrochemical system (CHI660D, CH Instruments, Shanghai, China) with an Ag/AgCl (in saturated KCl) as the reference electrode, a modified electrode as the working electrode and a platinum wire as the counter electrode. The DPV were carried out in the ranges of 0.6–1.2 V for guanine, 0.8–1.4 V for adenine, 0.4–1.4 V for mixture of guanine and adenine (increment: 0.004 V; amplitude: 0.05 V; pulse width: 0.2 s; sampling width: 0.02; pulse period: 0.5 s; quiet time: 2 s). All experiments were operated at ambient temperature.

Preparation of nanomaterials

According to Yang's method [17], IL-GR was synthesized through an epoxide ring-opening reaction between the 1-(3-aminopropyl)-3-methylimidazolium bromide (IL-NH₂) and GO. The IL-NH₂ was prepared according to the previous method [25]. The mechanism was shown in Scheme S1. MnO₂ nanosheets were prepared according to Mao's method [26]. The detailed preparation processes of IL-GR and MnO₂ nanosheets are given in the Electronic Supporting Material (ESM).

Fabrication of the modified electrodes

Firstly, the bare GCE was polished using γ -alumina with different particle sizes (0.3 and 0.05 μm) successively until a mirror-like surface was obtained. Then, after being washed using ethanol and water and dried in natural air, the pretreatment of GCE was completed. The IL-GR was mixed with MnO₂ nanosheets (1:1 volume ratio) and suffered ultrasonic to obtain a homogeneous MnO₂/IL-GR nanohybrid suspension. Next, 5 μL of the mixture was dripped onto the electrode surface by a pipette and dried naturally to acquire the MnO₂/IL-GR/GCE. MnO₂/GCE was obtained by the same drop coating method without IL-GR. Finally, the modified electrode was electropolymerized for 10 cycles by CV method in 0.1 M phosphate buffered solution (pH 8.5) containing 5 mM dopamine between - 0.6 V and +0.4 V to obtain PDA/MnO₂/IL-GR/GCE.

Actual sample treatment

Glucose citrate solution B (ACD): 0.48 g citric acid, 1.32 g sodium citrate and 1.47 g glucose were dissolved in 100 ml water and then sterilized.

Mouse fresh whole blood is obtained by taking from the eye socket. 0.7 mL of ACD solution was added into 5 mL of the freshly extracted blood and shocked rapidly. The above solution and the purchased FBS were stored at -20 °C.

Accurately removed 0.1 mL of fetal bovine serum (mice whole blood) with a pipette and diluted to 5 mL with BR buffer. DPV method was used to detect the guanine and adenine with different concentration in the above sample solution. The measurement conditions are shown in "Apparatus" section.

Results and discussion

Choice of materials

MnO₂ nanosheets possess chemical, electronic and electrochemical properties which are different properties than that of bulk. The higher surface energy and larger lateral surface

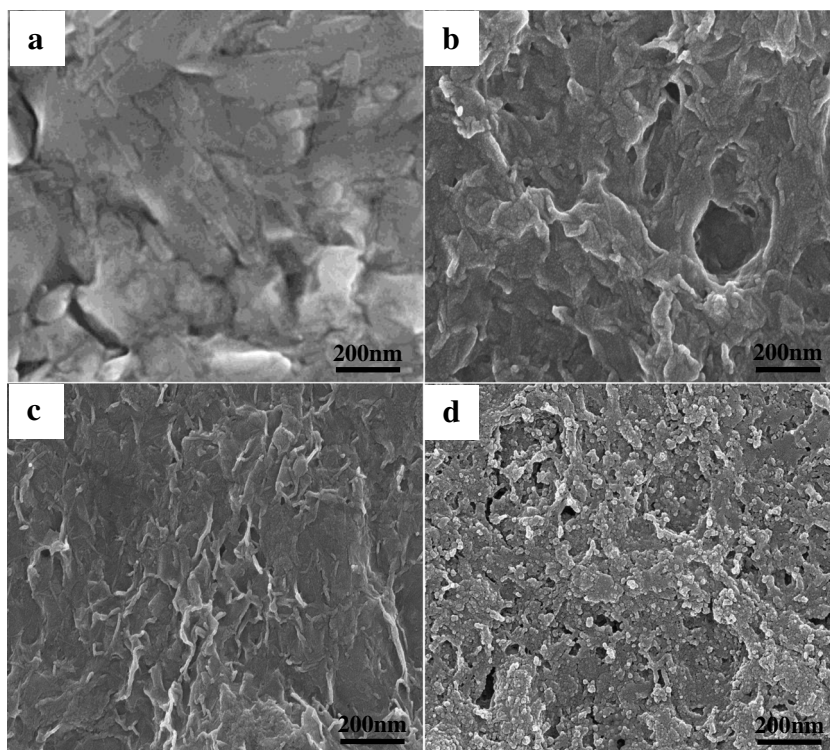
area provide additional site for electrochemical reaction. More importantly, with their unique two-dimensional structure, MnO₂ nanosheets are promising building blocks to form MnO₂-based nanocomposites with other structures. IL-GR solves the aggregation of graphene, and has good conductivity, polydispersity and stability. The positively charged IL-GR on the surface not only has stable dispersion and good electrical conductivity, but also can be better combined with negatively charged MnO₂ nanosheets to provide good sensing performances. In addition, the PDA membrane has a special selective permeability, which is expected to improve the selectivity of the electrochemical sensor after covered to the surface of the modified electrode.

Characterizations of the nanomaterials

SEM was employed to investigate the surface morphologies of various nanocomposites. Figure 1 shows typical SEM images of IL-GR, MnO₂ nanosheets, MnO₂/IL-GR and PDA/MnO₂/IL-GR. As shown in Fig. 1a, IL-GR exhibits a wrinkled structure, which is the characteristic of graphene. While a layered and flake-like structure can be observed distinctly for MnO₂ nanosheets in Fig. 1b. After being compounded together, MnO₂/IL-GR nanocomposites (Fig. 1c) show a uniform and lamellar fold structure, suggesting the successful combination of the materials. The structure of the composite was further studied by TEM as shown in (Fig. S1), which coincide with the results of SEM. Figure 1d exhibits the surface of the composite covered a thin layer of PDA. It can be clearly seen that PDA is a non-dense film, which not only ensures its selective permeability, but also does not hinder the electrocatalytic activity of MnO₂/IL-GR composites.

Figure 2a displays the Raman spectra of the MnO₂ nanosheets, IL-GR, and PDA/MnO₂/IL-GR. As can be seen from the Raman spectrum of IL-GR (b), there are two intense peaks around 1338 and 1595 cm^{-1} , which represent the D peak caused by structural defects in graphene and the G peak related to the first-order scattering of the E_{2g} phonons [27]. From the Raman spectrum of MnO₂ nanosheets (a), two Raman peaks are observed at 567 and 643 cm^{-1} due to the symmetric Mn-O vibrations [28]. While in the Raman spectrum of the nanocomposite, the characteristic peaks of MnO₂ nanosheets and IL-GR appear simultaneously indicating that the material is PDA/MnO₂/IL-GR. XPS was also executed to research the surface elemental composition and chemical states of PDA/MnO₂/IL-GR. The elements of C, N, O, Mn are detected in the entire nanocomposite materials (Fig. 2b). More specific results of XPS confirm the successful preparation of nanocomposites (Fig. S2). In addition, the elemental mapping images of MnO₂/IL-GR were acquired as shown in Fig. S3. It can be seen that C, Mn, N and O element are distributed throughout the nanostructure, which further confirm the successful synthesis of MnO₂/IL-GR.

Fig. 1 The typical SEM images of IL-GR (a), MnO₂ nanosheets (b), MnO₂/IL-GR (c) and PDA/MnO₂/IL-GR (d)



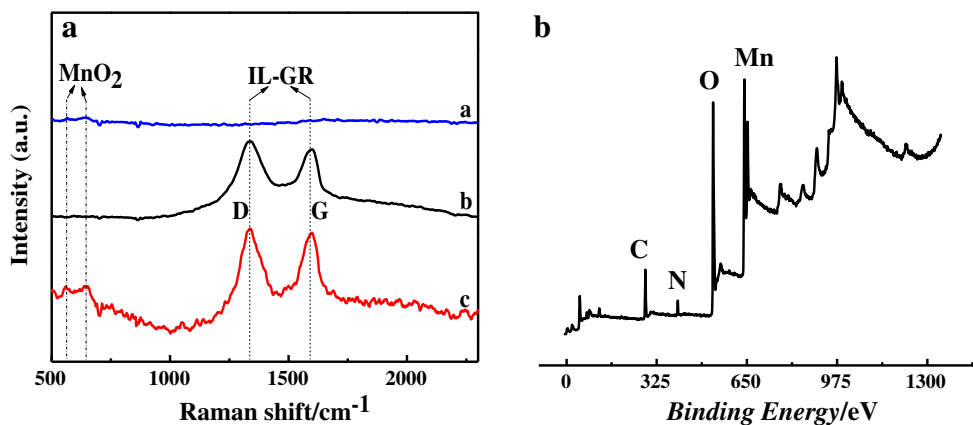
Electrochemical properties of modified electrodes

As is known, the semicircular portion at the higher frequency of electrochemical impedance spectrometry (EIS) can reveal the charge-transfer resistance (R_t) of modified materials and the R_t can be directly judged according to the diameter of semicircle [29]. Figure 3a shows a typical EIS pattern of various modified electrodes in 1 mM [Fe(CN)₆]^{3-/4-} solution (containing 0.1 M KCl). As can be seen from the results, compared with the bare GCE, the MnO₂/GCE exhibits a higher R_t , which may be because that the MnO₂ layer coated on the electrode surface blocks the electron transfer between interface and solution. While the electron transfer resistance at the interface of MnO₂/IL-GR/GCE significantly decrease than MnO₂/GCE, implying that the presence of IL-GR can significantly improve

the electroconductivity of the nanomaterials. In addition, the R_t on the PDA/MnO₂/IL-GR/GCE is slightly increased, which may be due to the electric insulativity of the PDA film [30].

In order to investigate the electrochemical behaviors of guanine and adenine on different modified electrodes, 300 μM of adenine and guanine in BR buffer (pH = 4) were detected by cyclic voltammetry (CV) method on various modified electrodes as shown in Fig. 3b–d. Obviously, compared with bare GCE (a) and MnO₂/GCE (b), MnO₂/IL-GR/GCE (c) exhibits the largest peak currents whether for the individual detections or the simultaneous detection of guanine and adenine. The reason may be that the large surface areas of MnO₂ nanosheets provide a large number of active sites, and the good conductivity of IL-GR reduces the electron transfer resistance. Since the good structure of composite is beneficial to

Fig. 2 a Raman spectra of (a) MnO₂ nanosheets, (b) IL-GR, and (c) PDA/MnO₂/IL-GR. b XPS spectra for the PDA/MnO₂/IL-GR



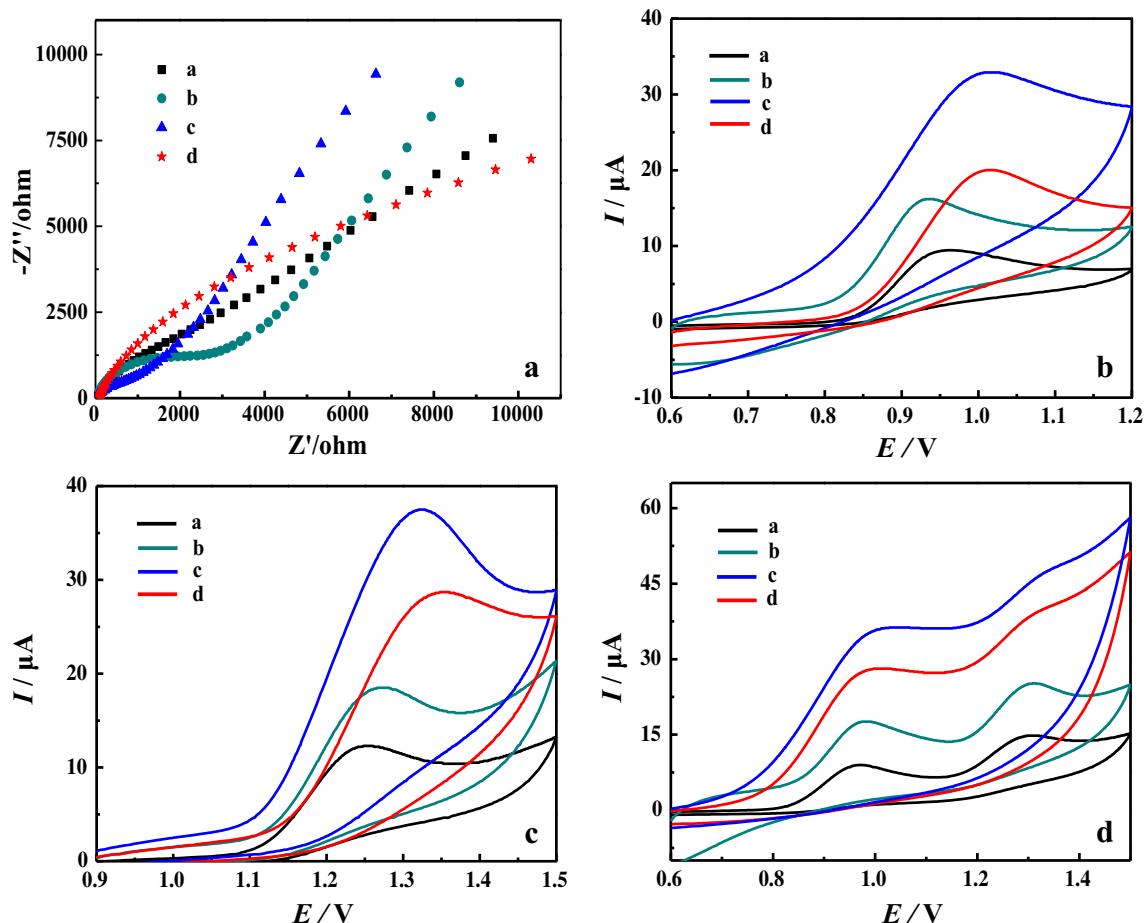


Fig. 3 a EIS of (a) bare GCE, (b) MnO_2/GCE , (c) IL-GR/ MnO_2/GCE and (d) PDA/IL-GR/ MnO_2/GCE in a 5 mM $[\text{Fe}(\text{CN})_6]^{3-/4-}$ containing 0.1 M KCl. CV responses of (a) bare GCE, (b) MnO_2/GCE , (c) $\text{MnO}_2/\text{IL-GR}/\text{GCE}$

IL-GR/ GCE and (d) PDA/IL-GR/ MnO_2/GCE in BR buffer (pH = 4.0) containing 300 μM of (b) guanine, (c) adenine, (d) mixture of guanine and adenine at a scan rate of 100 mV s^{-1}

improve mass transfer efficiency and electrical activity of the electrode, after being covered with PDA, there is still a good response current on the modified electrode. Besides, for the simultaneous detection, the peak-to-peak separation of the two kinds of purines is more than 300 mV, which is large enough to detect both guanine and adenine without any interference between them. This result suggests that the synergistic effect of MnO_2 and IL-GR with PDA film can significantly improve the catalytic activity toward the guanine and adenine.

As shown in Fig. S4, CV method was performed to investigate the oxidation kinetics of guanine and adenine on the PDA/ $\text{MnO}_2/\text{IL-GR}/\text{GCE}$ at different scan rates. It can be found that the oxidation peak currents of guanine and adenine (150 μM) increase gradually in the ranges of 100–1000 mV s^{-1} . Moreover, there are linearities between the oxidation peak currents and the square root of the scan rates ($v^{1/2}$), and the fitted regression equations are $I = 52.849v^{1/2} - 167.56$ ($R^2 = 0.9915$) and $I = 5.4864 v^{1/2} + 1.9768$ ($R^2 = 0.9982$) for the detection of guanine and adenine, respectively. In simultaneous detection, the regression equations are $I = 2.0663 v^{1/2} + 50.798$ ($R^2 = 0.9867$) and $I = 6.0436 v^{1/2} + 109.419$ ($R^2 =$

0.9756) for guanine and adenine, separately. These results indicate that the electrochemical oxidation of guanine and adenine on PDA/ $\text{MnO}_2/\text{IL-GR}/\text{GCE}$ are diffusion-controlled processes [31]. It can be concluded that the oxidation reactions of guanine and adenine are absolutely irreversible processes as only the oxidation peaks are observed.

Moreover, as the scan rates increase, the oxidation peak potential (E_p) shifts positively. In Fig. S4A and B, the corresponding equations are $E_p = 0.0813 \log v + 0.8204$ ($R^2 = 0.9782$) and $E_p = 0.0993 \log v + 1.0155$ ($R^2 = 0.9932$), respectively. According Laviron equation:

$$E_p = E^o + (RT/\alpha nF) \ln(RT k_s / \alpha nF) + (RT/\alpha nF) \lg v$$

where E^o represents the formal redox potential, R is molar gas constant (8.314 $\text{J K}^{-1} \text{mol}^{-1}$), T is temperature (298 K), k_s is the standard rate constant of the reaction, α is the transfer coefficient (which can be assumed to be 0.5) and F is Faraday's constant (96,480 C mol^{-1}). The number of electron transferred (n) in the processes controlled by diffusion can be calculated to be 0.63 for guanine and 0.52 for adenine.

As protons always take part in the oxidation reactions and have a significant effect on the reaction rate, the effect of pH on the electrochemical behavior of guanine and adenine was also studied. The DPV characterizations of the 150 μM guanine, adenine, and their mixture were performed in BR solution with different pH (3.0–8.0). The oxidation reactions of both guanine and adenine are significantly affected by pH as shown in Fig. 4. For the guanine, the highest oxidation peak current is present at pH=4.0, while for the adenine, pH=3.0. For the simultaneous detection, the oxidation currents of guanine and adenine reach peak value maximum concurrently at pH=3.0, but have a large background current as shown in Fig. 4c. Therefore, in order to obtain a lower detection limit, pH=4.0 was chosen as the optimal acidity condition. In addition, due to the reaction between protons and the electrode, the oxidation peak potential shifts negatively with increasing pH, showing a good linear relationship between peak potential (E_p) and pH. In the individual detection, E_p (V) = $-0.0398 \text{ pH} + 1.0245$ ($R^2 = 0.9912$) was obtained for

guanine, and E_p (V) = $-0.0530 \text{ pH} + 1.3989$ ($R^2 = 0.9888$) was obtained for adenine. In the simultaneous detection, E_p (V) = $-0.0625 \text{ pH} + 1.3951$ ($R^2 = 0.9910$) and E_p (V) = $-0.0458 \text{ pH} + 1.0163$ ($R^2 = 0.9930$) were get for guanine and adenine, respectively. According to the Nernst equation, when the pH increase one unit, the potential shift of guanine (-62 mV) and adenine (-46 mV) indicates the corresponding amount of electron transfer coupled with proton transfer [32]. The electro-oxidation mechanism of guanine and adenine is shown in Fig. 4d [33].

Under the optimal experimental conditions, the electrochemical behavior of guanine and adenine on PDA/MnO₂/IL-GR/GCE was estimated by DPV method. As shown in Fig. 5, in the concentration ranges of 10–300 μM , the oxidation peak currents of guanine and adenine increase along with the increasing of concentration, and reach the peak currents at about +0.80 V and +1.16 V, respectively. In the individual detection, the relationship between the peak current (I_p) and concentration of guanine can be fitted to a linear regression equation of I_p (μA) = $0.0159c$ (μM) +

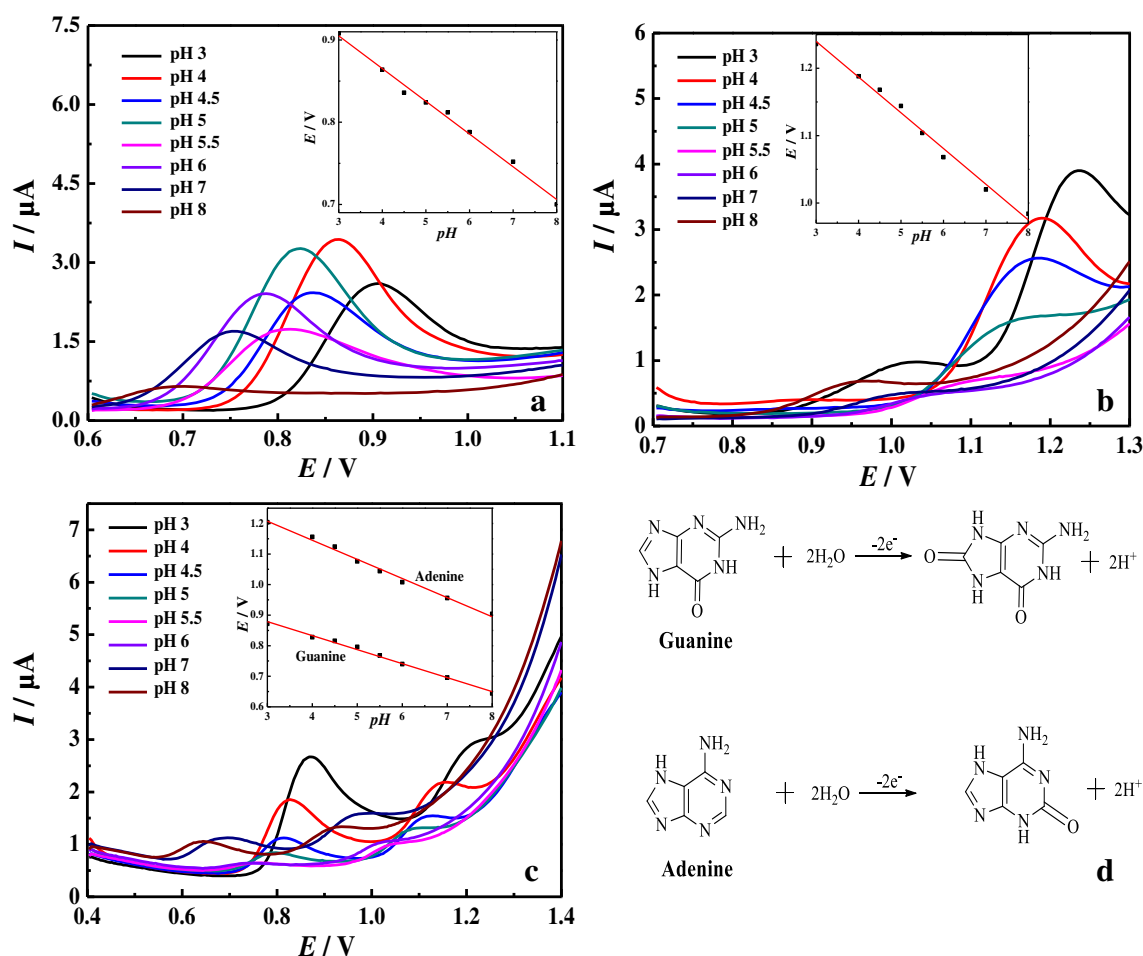


Fig. 4 DPV responses of PDA/MnO₂/IL-GR/GCE in BR buffer with different pH values from 3.0 to 8.0, containing 150 μM of (a) guanine, (b) adenine, (c) mixture of guanine and adenine. The scan rate was

100 mV s^{-1} . The inset: Plots of the peak potential vs. the pH. **d** The electro-oxidation mechanism of guanine and adenine

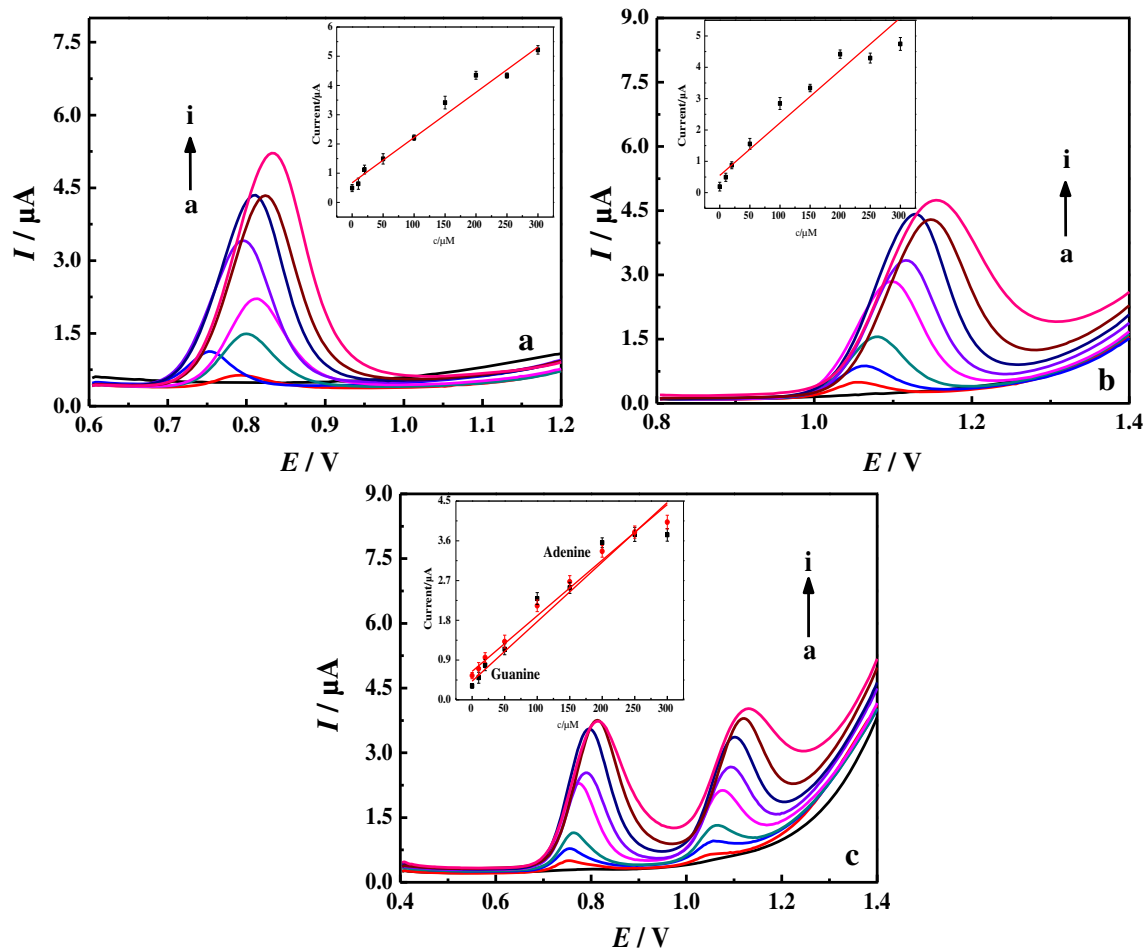


Fig. 5 DPV responses of PDA/MnO₂/IL-GR/GCE in BR buffer (pH = 4.0) with increasing the concentrations of (a) guanine, (b) adenine, (c) mixture of guanine and adenine. a to i correspond to 0, 10, 20, 50, 100,

150, 200, 250, 300 μM, respectively. The scan rate was 100 mV s⁻¹. The inset: Plots of the peak current vs. the concentrations

0.6814 ($R^2 = 0.9725$), with a detection limit of 0.18 μM ($S/N = 3$). The DPV plots of adenine can be fitted to a linear regression equation of I_p (μA) = 0.0156c (μM) + 0.6551 ($R^2 = 0.9250$) with a detection limit of 0.22 μM ($S/N = 3$). In the simultaneous detection, the calibration curves for guanine and adenine exhibit a linear regression equation as I_p (μA) = 0.0122 c (μM) + 0.6145 ($R^2 = 0.9370$) for

guanine; I_p (μA) = 0.0118 c (μM) + 0.7812 ($R^2 = 0.9811$) for adenine, and the detection limits are 0.25 and 0.15 μM ($S/N = 3$), respectively. In addition, our work was compared with some other electrochemical sensors that detected guanine and adenine simultaneously. The data in Table 1 indicates that the sensor in this work concurrently possesses lower detection limits and a wider linear range.

Table 1 Comparison with some other electrochemical sensors that detected guanine and adenine simultaneously

Sensors	Methods	Detection limit (μM)		Linear range (μM)		References
		guanine	adenine	guanine	adenine	
PPDA/CRGO/GCE	DPV	0.01	0.02	0.05–4.5	0.1–6.0	[9]
ERCGr/GCE	DPV	0.15	0.10	0.5–10	2.5–50	[10]
MWCNTs/NiFe ₂ O ₄ /GCE	LSV	0.006	0.01	0.05–3.0	0.1–4.0	[11]
Cu@Ni/MWCNTs	DPV	0.35	0.56	5.0–150	8.0–150	[33]
CQD/PAPox/GCE	DPV	0.51	0.39	1.0–65	2.0–70	[34]
f-DNPs/CS/GCE	DPV	0.002	0.01	0.05–30	0.1–14	[35]
PDA/MnO ₂ /IL-GR/GCE	DPV	0.25	0.15	10–300		This work

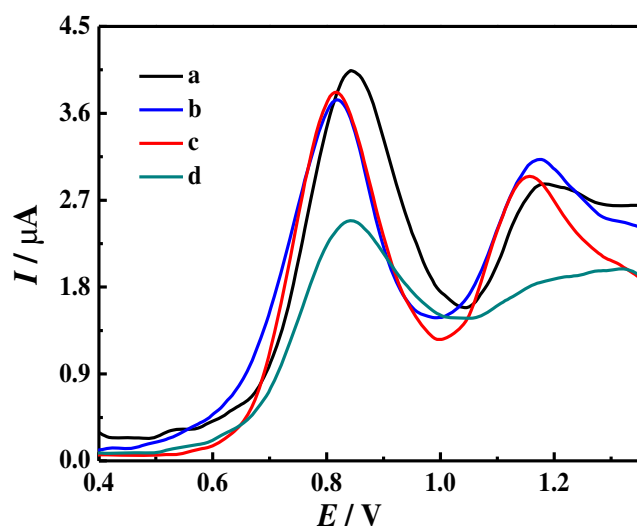


Fig. 6 DPV responses of (a) $\text{MnO}_2/\text{IL-GR}/\text{GCE}$, (c) $\text{PDA}/\text{IL-GR}/\text{MnO}_2/\text{GCE}$ and after immersion in 50 mg mL^{-1} BSA solution (b) $\text{MnO}_2/\text{IL-GR}/\text{GCE}$, (d) $\text{PDA}/\text{IL-GR}/\text{MnO}_2/\text{GCE}$ in BR buffer (pH = 4.0) containing $300 \mu\text{M}$ mixture of guanine and adenine at a scan rate of 100 mV s^{-1}

Anti-fouling performance, selectivity and reproducibility

Taking a single protein BSA solution of 50 mg mL^{-1} as an example, the anti-pollution performance of $\text{PDA}/\text{MnO}_2/\text{IL-GR}/\text{GCE}$ was explored in detail by DPV method, as shown in Fig. 6. It can be seen from the experimental results that the current on the $\text{MnO}_2/\text{IL-GR}/\text{GCE}$ is greatly reduced (a and b). The electrochemical response of the $\text{PDA}/\text{MnO}_2/\text{IL-GR}/\text{GCE}$ (c and d) has no significant change after immersion in the BSA solution for 30 min, indicating that $\text{PDA}/\text{MnO}_2/\text{IL-GR}/\text{GCE}$ has an excellent ability to eliminate the non-specific adsorption of a single protein. The results confirm that $\text{PDA}/\text{MnO}_2/\text{IL-GR}$ can be used in the preparation of anti-pollution biosensors to improve the selectivity and sensitivity of detection.

Table 2 Recoveries for the simultaneous determination of guanine and adenine in FBS and mice whole blood samples ($n = 5$)

Blood sample		Spiked (μM)	Found (μM)	Recovery (%)	RSD (%)
FBS	Guanine	10	10.44	104.4	0.9
		50	52.78	105.6	3.1
		100	95.20	95.2	1.7
	Adenine	10	10.49	104.9	2.3
		50	47.91	95.8	1.1
		100	102.3	102.3	2.7
Mice whole blood	Guanine	10	9.32	93.2	3.3
		50	45.56	91.1	2.6
		100	92.12	92.1	3.7
	Adenine	10	8.57	85.7	4.1
		50	48.32	96.6	2.1
		100	103.8	103.8	4.9

To further evaluate the selectivity of the modified electrode for guanine and adenine detection, the interference detection of several coexisting substances such as UA, AA, NaCl and glucose were assessed on $\text{PDA}/\text{MnO}_2/\text{IL-GR}/\text{GCE}$. When the relative error (E_r) is less than 5%, the tested substance is considered no interfering on major constituents. As shown in Fig. S5A, $\text{PDA}/\text{MnO}_2/\text{IL-GR}/\text{GCE}$ has good selectivity for the simultaneous detection of guanine and adenine. The reproducibility of $\text{PDA}/\text{MnO}_2/\text{IL-GR}/\text{GCE}$ was studied by detecting the guanine and adenine ($150 \mu\text{M}$) using six modified electrodes modified electrode based on the same fabrication procedure (Fig. S5B). The RSD of 3.7% for guanine and 4.1% for adenine demonstrate an excellent reproducibility of $\text{PDA}/\text{MnO}_2/\text{IL-GR}/\text{GCE}$.

Real sample analysis

To assess the application of this method in actual samples, the $\text{PDA}/\text{MnO}_2/\text{IL-GR}/\text{GCE}$ was applied to the determination of guanine and adenine in FBS and mice whole blood samples using standard addition method. The sample solutions were diluted 50-fold with BR buffer and stored at $-4 \text{ }^\circ\text{C}$. Then, 10, 50, and $100 \mu\text{M}$ guanine and adenine standard solutions were added into the stock solutions and detected using the modified electrode. As shown in Table 2, the recoveries from 85.7% - 105.6% suggest that $\text{PDA}/\text{MnO}_2/\text{IL-GR}/\text{GCE}$ can be used commendably for simultaneous detection of guanine and adenine in blood samples.

Conclusions

An electrochemical sensor based on $\text{PDA}/\text{MnO}_2/\text{IL-GR}$ was constructed for the determination of guanine and adenine. The results showed that $\text{PDA}/\text{MnO}_2/\text{IL-GR}/\text{GCE}$ exhibited good electrochemical performance, low detection limits, wide linear range, good selectivity and reproducibility, which were attributed to the synergy of $\text{MnO}_2/\text{IL-GR}$ and PDA film. The utility of the sensor for the detection of guanine and adenine in fetal bovine serum and mouse whole blood has been preliminarily verified. This work provides a new idea for the simultaneous detection of guanine and adenine in blood samples which is expected to be applied in a wider range of electrochemical fields. In addition, the applicability and accuracy of this sensor for more actual samples needs further verification.

Acknowledgments This work was financially supported by the National Natural Science Foundation of China (21778047, 21675138), and the Department of Science and Technology of Shandong Province of China (No. 2018GSF116011, GG201709290055) and of Yantai City of China (No. 2017ZH093).

Compliance with ethical standards There are no conflicts to declare.

References

- Wang H, Zhang H, Xu L, Gan T, Huang K, Liu Y (2014) Electrochemical biosensor for simultaneous determination of guanine and adenine based on dopamine-melanin colloidal nanospheres-graphene composites. *J Solid State Electrochem* 18(9):2435–2442
- Li S, Li P, Dong T, Tsim K (2015) Determination of nucleosides in natural *Cordyceps sinensis* and cultured *Cordyceps mycelia* by capillary electrophoresis. *Chin J Pharm Anal* 22(1):144–150
- Ibrahim H, Temerk Y, Farhan N (2016) Electrochemical sensor for individual and simultaneous determination of guanine and adenine in biological fluids and in DNA based on a nano-in-ceria modified glassy carbon paste electrode. *RSC Adv* 6(93):90220–90231
- Yang F, Guan J, Li S (2007) Fast simultaneous determination of 14 nucleosides and nucleobases in cultured cordyceps using ultra-performance liquid chromatography. *Talanta* 73(2):269–273
- Thomas B, Matson S, Chopra V, Sun L, Sharma S, Hersch S, Rosas H, Scherzer C, Ferrante R, Matson W (2013) A novel method for detecting 7-methyl guanine reveals aberrant methylation levels in Huntington disease. *Anal Biochem* 436(2):112–120
- Lin H, Xu D, Chen H (1997) Simultaneous determination of purine bases, ribonucleosides and ribonucleotides by capillary electrophoresis-electrochemistry with a copper electrode. *J Chromatogr A* 760(2):227–233
- Huang Y, Chang H (2007) Analysis of adenosine triphosphate and glutathione through gold nanoparticles assisted laser desorption/ionization mass spectrometry. *Anal Chem* 79(13):4852–4859
- Rezaei B, Khosropour H, Ensafi A, Dinari M, Nabiyan A (2015) A new electrochemical sensor for the simultaneous determination of guanine and adenine: using a NiAl-layered double hydroxide/graphene oxide-multi wall carbon nanotube modified glassy carbon electrode. *RSC Adv* 5(92):75756–75765
- Li C, Qiu X, Ling Y (2013) Electrocatalytic oxidation and the simultaneous determination of guanine and adenine on (2,6-pyridinedicarboxylic acid)/graphene composite film modified electrode. *J Electroanal Chem* 704(6):44–49
- Xu J, Li T, Shen S, Zhao L, Ma C, Mahmoud AE, Wang J (2015) Electrochemically reduced carboxyl graphene modified electrode for simultaneous determination of guanine and adenine. *Anal Lett* 48(9):1465–1480
- Ensafi A, Jafari-Asl M, Rezaei B, Allafchian A (2013) Simultaneous determination of guanine and adenine in DNA based on NiFe₂O₄ magnetic nanoparticles decorated MWCNTs as a novel electrochemical sensor using adsorptive stripping voltammetry. *Sensors Actuators B Chem* 177(1):634–642
- Wang H, Li S, Si Y, Zhang N, Sun Z, Wu H, Lin Y (2014) Platinum nanocatalysts loaded on graphene oxide-dispersed carbon nanotubes with greatly enhanced peroxidase-like catalysis and electrocatalysis activities. *Nanoscale* 6(14):8107–8116
- Dong M, Liu C, Li S, Li R, Qiao Y, Zhang L, Wei W, Qi W, Wang H (2016) Polymerizing dopamine onto Q-graphene scaffolds towards the fluorescent nanocomposites with high aqueous stability and enhanced fluorescence for the fluorescence analysis and imaging of copper ions. *Sensors Actuators B Chem* 232:234–242
- Cai Y, Feng L, Hua Y, Liu H, Yin M, Lv X, Li S, Wang H (2018) Q-graphene-loaded metal organic framework nanocomposites with water-triggered fluorescence turn-on: fluorimetric test strips for directly sensing trace water in organic solvents. *Chem Commun* 54(96):13595–13598
- Hua Y, Li S, Cai Y, Liu H, Wan Y, Yin M, Wang F, Wang H (2019) A sensitive and selective electroanalysis strategy for histidine using the wettable well electrodes modified with graphene quantum dot-scaffolded melamine and copper nanocomposites. *Nanoscale* 11(5):2126–2130
- Luan F, Zhang S, Chen D, Zheng K, Zhuang X (2018) CoS₂-decorated ionic liquid-functionalized graphene as a novel hydrazine electrochemical sensor. *Talanta* 182:529–535
- Yang H, Shan C, Li F, Han D, Zhang Q, Niu L (2009) Covalent functionalization of polydisperse chemically-converted graphene sheets with amine-terminated ionic liquid. *Chem Commun* 45(26):3880–3882
- Shan C, Yang H, Han D, Zhang Q (2010) Electrochemical determination of NADH and ethanol based on ionic liquid-functionalized graphene. *Biosens Bioelectron* 25(6):1504–1508
- Yang W, Gao Z, Wang J, Wang B, Liu Q, Li Z, Mann T, Yang P, Zhang M, Liu L (2012) Synthesis of reduced graphene nanosheet/urchin-like manganese dioxide composite and high performance as supercapacitor electrode. *Electrochim Acta* 69(5):112–119
- Wang X, Luo C, Li L, Duan H (2015) Highly selective and sensitive electrochemical sensor for L-cysteine detection based on graphene oxide/multiwalled carbon nanotube/manganese dioxide/gold nanoparticles composite. *J Electroanal Chem* 757:100–106
- Xu H, Zhang W (2017) Graphene oxide-MnO₂ nanocomposite-modified glassy carbon electrode as an efficient sensor for H₂O₂. *Chin Chem Lett* 28(1):143–148
- Indrani B, Pangule R, Kane R (2011) Antifouling coatings: recent developments in the design of surfaces that prevent fouling by proteins, bacteria, and marine organisms. *Adv Mater* 23(6):690–718
- Li Y, Su Y, Zhao X, He X, Zhang R, Zhao J, Fan X, Jiang Z (2014) Antifouling, high-flux nanofiltration membranes enabled by dual functional polydopamine. *ACS Appl Mater Interfaces* 6(8):5548–5557
- Li R, Liu X, Qiu W, Zhang M (2016) In vivo monitoring of H₂O₂ with polydopamine and prussian blue-coated microelectrode. *Anal Chem* 88(15):7769–7776
- Hu Y, Hua S, Li F, Jiang Y, Bai X, Li D, Niu L (2011) Green-synthesized gold nanoparticles decorated graphene sheets for label-free electrochemical impedance DNA hybridization biosensing. *Biosens Bioelectron* 26(11):4355–4361
- Zhai W, Wang C, Yu P, Wang Y, Mao L (2014) Single-layer MnO₂ nanosheets suppressed fluorescence of 7-Hydroxycoumarin: mechanistic study and application for sensitive sensing of ascorbic acid in vivo. *Anal Chem* 86(24):12206–12213
- Chen S, Zhu J, Wu X, Han Q, Wang X (2010) Graphene oxide–MnO₂ nanocomposites for supercapacitors. *ACS Nano* 4(5):2822–2830
- Gao T, Glerup M, Krumeich F, Nesper R, Fjellvåg H, Norby P (2008) Microstructures and spectroscopic properties of cryptomelane-type manganese dioxide nanofibers. *J Phys Chem C* 112(34):13134–13140
- Guo H, Wang X, Qian Q, Wang F, Xia X (2009) A green approach to the synthesis of graphene nanosheets. *ACS Nano* 3(9):2653–2659
- Li Y, Liu M, Xiang C, Xie Q, Yao S (2006) Electrochemical quartz crystal microbalance study on growth and property of the polymer deposit at gold electrodes during oxidation of dopamine in aqueous solutions. *Thin Solid Films* 497(1–2):270–278
- Yang Z, Zheng X, Zheng J (2017) Facile synthesis of three-dimensional porous Au@Pt core-shell nanoflowers supported on graphene oxide for highly sensitive and selective detection of hydrazine. *Chem Eng J* 327:431–440
- Wang S, Xu Q (2007) Electrochemical parameters of ethamsylate at multi-walled carbon nanotube modified glassy carbon electrodes. *Bioelectrochemistry* 70(2):296–300

33. Wang D, Huang B, Liu J, Guo X, Abudukeyoumu G, Zhang Y, Ye B, Li Y (2017) A novel electrochemical sensor based on Cu@Ni/MWCNTs nanocomposite for simultaneous determination of guanine and adenine. *Biosens Bioelectron* 102:389–395
34. He S, He P, Zhang X (2018) Simultaneous voltammetric determination of guanine and adenine by using a glassy carbon electrode modified with a composite consisting of carbon quantum dots and overoxidized poly(2-aminopyridine). *Microchim Acta* 185(2):107
35. Habibi B, Jahanbakhshi M (2016) A glassy carbon electrode modified with carboxylated diamond nanoparticles for differential pulse voltammetric simultaneous determination of guanine and adenine. *Microchim Acta* 183(7):2317–2325

Publisher's note Springer Nature remains neutral with regard to jurisdictional claims in published maps and institutional affiliations.